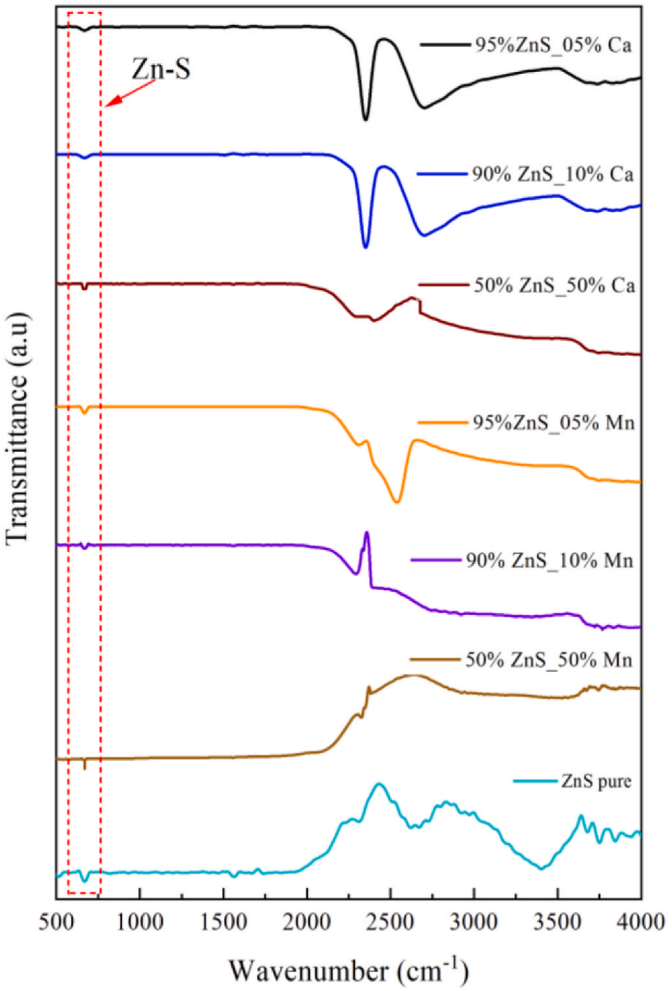


Fig. 13. Ftir spectra of ZnS pure and Mn/Ca doped thin films at different concentrations.

has a significant influence on the morphological properties of the films more than doping with Mn. Ca doping has increased the surface roughness of ZnS thin films as presented in Table 2. This is due to the fact that Ca ions are larger than Zn ions, and their incorporation into the lattice of ZnS can create defects and distortions, leading to an increase in surface roughness. Ca doping has affected the surface morphology of ZnS thin films, resulting in the formation of different surface structures, as Fig. 6 shows. Samples with high Mn content exhibit a distinct behavior, as depicted in Fig. 6 (a). During the evaporation process, Mn atoms migrate towards the substrate and coalesce, leading to the formation of agglomerates. These agglomerates contribute to the roughness of the resulting film, with some of them reaching a size of 456 nm.

The AFM is a powerful imaging technique that allows scientists to visualize the surface of materials at the nanoscale level [48]. Minkowski analysis is a mathematical approach that can be used to extract quantitative information about the surface topology from AFM images. In Minkowski analysis, the surface of the material is treated as a geometric object, and a set of mathematical descriptors called Minkowski functionals are used to characterize the shape and structure of the surface. These functionals provide information about the surface area, volume, curvature, and other geometric properties of the material [49]. In this study, Minkowski functions were used for the analysis of the AFM of the developed samples as illustrated in Figs. 9–11.

The Minkowski surface area function describes the total area of the surface. The Minkowski volume function describes the amount of space enclosed by the surface. Wille the Minkowski connectivity analysis can be a valuable tool for understanding the porous structure of thin films and optimizing their performance in various applications. Undoped ZnS presents the highest maximum of surface and connectivity while the sample with 50% of Ca has the largest total surface area with the amount of space enclosed by the surface with a more porous structure presenting the lower maximum. The other films covered smaller areas than ZnS and the maximum increases with increasing ZnS in the structure. The obtained results confirm that doping influences the morphological properties of thin films.

Fig. 12 represents optical images of pure ZnS thin films and ZnS thin films doped with varying concentrations of Mn and Ca elements. The optical images reveal alterations in the surface structure of the ZnS thin films due to the doping process, aligning with the results obtained from AFM measurements.

3.2. FTIR spectroscopy

In this investigation, FTIR analyses demonstrated the presence of ZnS and identified additional functional groups on the surfaces of the thin films. The infrared spectrum of the investigated thin films, displayed in Fig. 13, was recorded across wavelengths ranging from 500 to 4000 cm^{-1}. While all prepared films demonstrated similar FTIR spectra, slight shifts in peak positions were noticeable. These slight shifts towards lower wave numbers are likely attributed to the incorporation of Mn^{2+} and Ca^{2+} ions into the ZnS crystal lattice. Fig. 13 illustrates weak

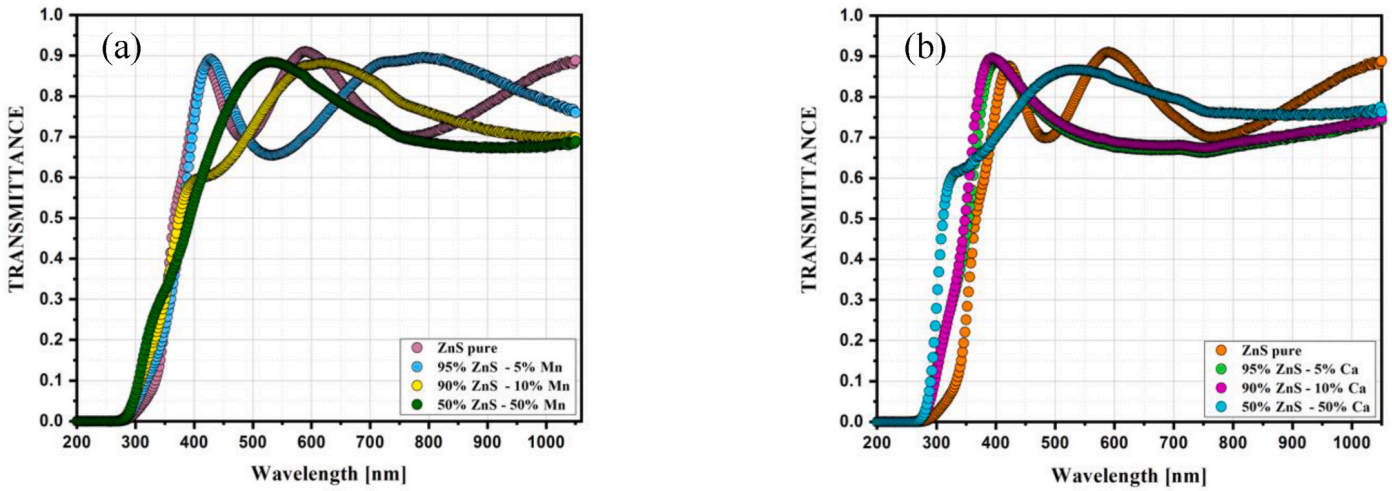


Fig. 14. Transmittance spectra of (a) ZnS–Mn thin films (b) ZnS–Ca thin films.

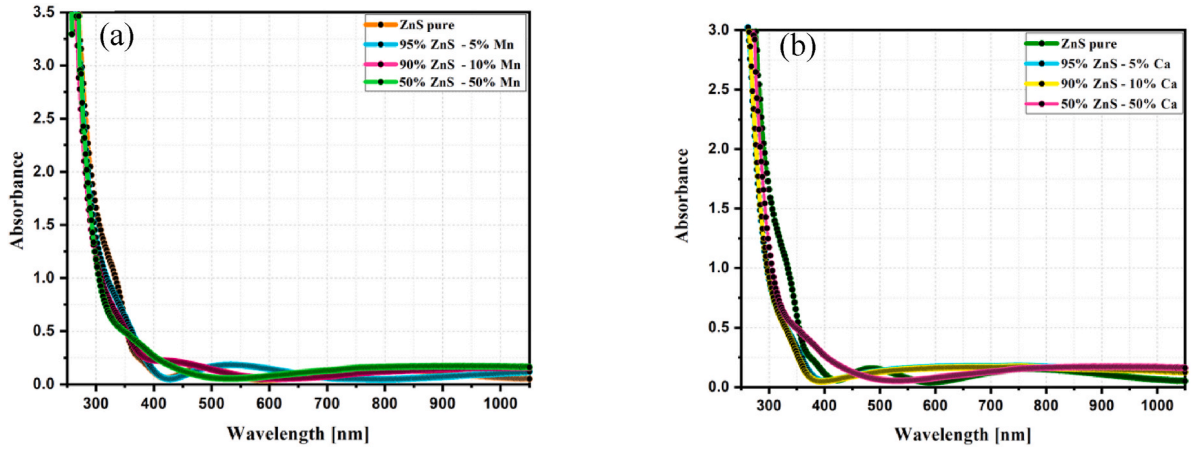


Fig. 15. Absorbance spectra of (a) ZnS–Mn thin films (b) ZnS–Ca thin films.

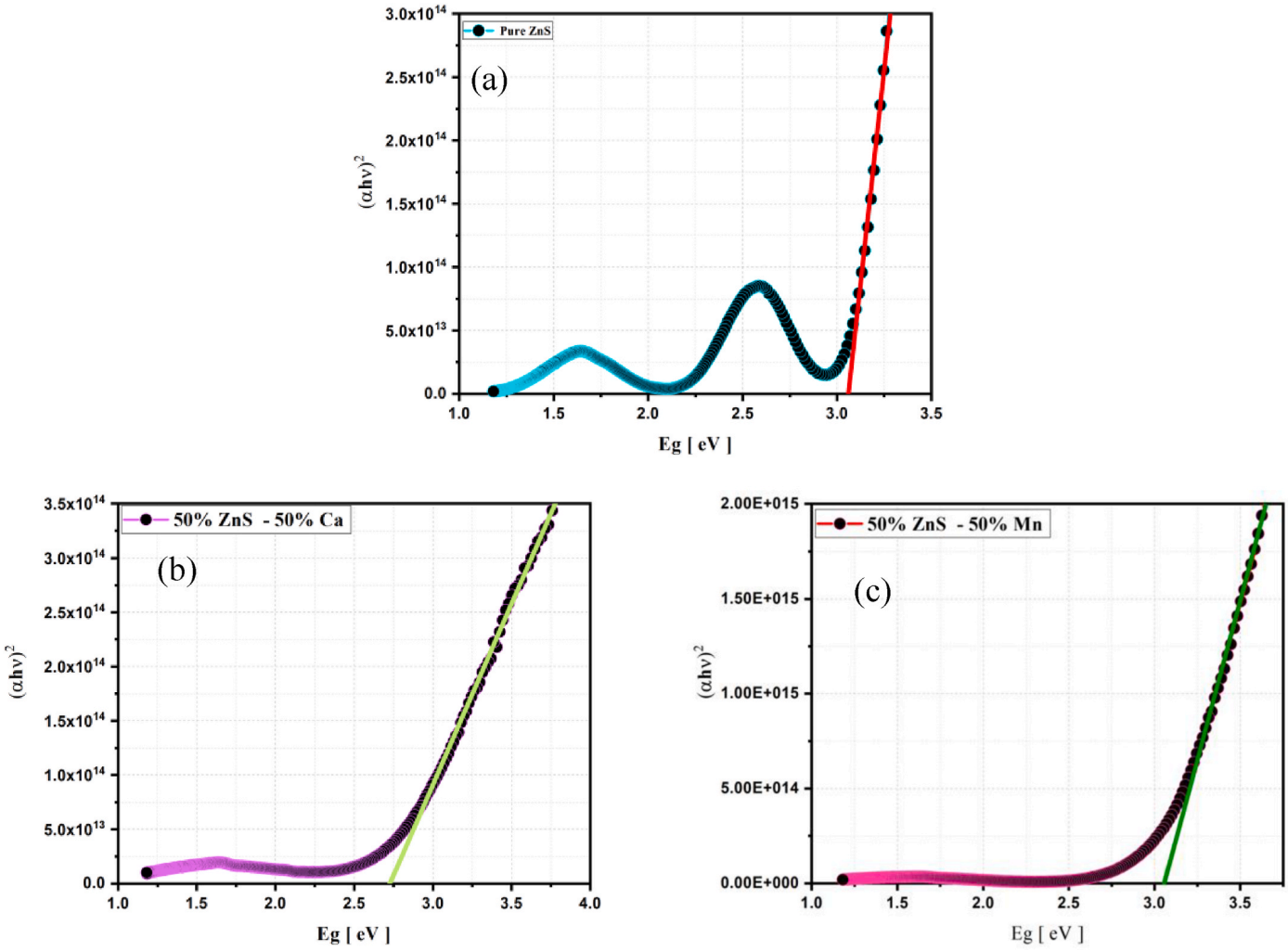


Fig. 16. Variation of $(\alpha E)^2$ for (a) Undoped ZnS Thin film, (b) 50% ZnS_50% Ca thin film, and (c) 50% ZnS_50% Mn thin film.

characteristic vibrations of zinc sulfide at 669 cm^{-1} [50–54]. Furthermore, the additional peaks are associated with the C═O stretching mode, originating from the absorption of atmospheric CO_2 on the film surface, and can be attributed to carboxyl (C═O) and methylene groups.

3.3. Optical properties

3.3.1. Transmittance

The optical transmittance spectra of ZnS–Mn and ZnS–Ca thin films at various Mn and Ca doping levels (5%, 10%, and 50%) were measured at room temperature in the range of 200–1100 nm as shown in Fig. 14. The samples presented a high transmittance of approximately 70%–90%

Table 3
The table groups the values of gap energies obtained by the Tauc plot method for all samples.

	Pure ZnS	ZnS 95% _ X 5%		ZnS 90% _ X 10%		ZnS 50% _ X 50%	
		X = Mn	X = Ca	X = Mn	X = Ca	X = Mn	X = Ca
Eg [eV]	3.05	3.14	3.08	3.14	3.14	3.05	2.79

in the wavelength range of 400 to 110 nm for pure ZnS, and in the wavelength range of 500 nm–1100 nm for the samples doped Mn. While the samples doped by Ca, presented a transmittance of approximately 60%–90% in the range 350 nm–110 nm which is considerably greater than reported by literature [55–57]. These properties make this composition a suitable candidate not only for solar cells but also for other optoelectronic devices and they can also be used in CIGS solar cells in place of CdS.

The transmission spectra of pure ZnS and Mn-doped ZnS samples showed interference bangs. These observed bangs can be attributed to the interference between the air-film reflected waves and the film-substrate interfaces which are glass in our case. While samples doped of Ca exhibit an absence of interference bangs in the transmission spectra due to low multiple reflections at the interface. And also represents a diminishing of transmittance as the doping concentration increases, this diminishing of transmittance in these samples can be attributed to the increase in scattered light intensity due to the higher surface roughness. These findings are in good agreement with the reported literature and the results of AFM analysis.

As shown in Fig. 15, the UV–Vis absorption spectra of ZnS thin films doped by Mn and Ca were also measured in the range of 250–1100 nm. The ZnS–Ca samples demonstrated a slight shift of the absorption edges to a higher wavelength, which would strongly influence the band gap of the ZnS thin films by the Ca doping. For ZnS–Mn samples, the absorption edges are approximately on the same point as for pure ZnS film. Generally, all the thin films exhibited a high absorbance for wavelengths below 350 nm and a low value for wavelengths over 350 nm. This property implies that ZnS–Ca and ZnS–Mn thin films are a good alternative as a window layer for solar cells.

The optical band gap values (E_g) of ZnS–Ca and ZnS–Mn thin films were estimated using the Tauc equation which is given by.

$$(\alpha h\nu)^{1/n} = k(E - E_g) \quad (1)$$

$$\alpha = A/0,4343 * d \quad (2)$$

$$A = -log\,(T) \quad (3)$$

Where α is the linear absorption coefficient, k is a parameter that depends on the transition probability, h is Planck's constant, ν is the frequency, and E_g is the optical band. n is a parameter that depends on the nature of the transition and is equal to ½ for a direct transition allowed.

As shown in Fig. 16, the optical band gap energy of ZnS–Mn and ZnS–Ca thin films was determined. Table 3 summarizes the results obtained.

It is observed that the band gap value E_g decreases from 3.05 to 2.7 eV by increasing the concentration of Ca doping and it remains approximately the same at 3.1 eV by varying the doping of Mn. This diminution of the band gap energy value for ZnS–Ca can be attributed to the decrease in the number of grain boundaries as a result of the increase in the crystalline size of the films. While ZnS–Mn samples, the value remains the same and is attributed to the atomic properties of the element Mn which are close to Zn. However, we can report that the Ca doping is much more effective than the Mn dopant in decreasing the optical band gap value.

Therefore, pure ZnS thin films exhibit a narrow bandgap energy of approximately 3.05 eV. However, there are instances in the literature, such as the study referenced [58–60] reporting slightly higher bandgap energy of 3.2 eV for pure ZnS. This finding resonates more closely with our observations. Our deposition method, carried out through physical vapor deposition under high vacuum, inherently imparts unique

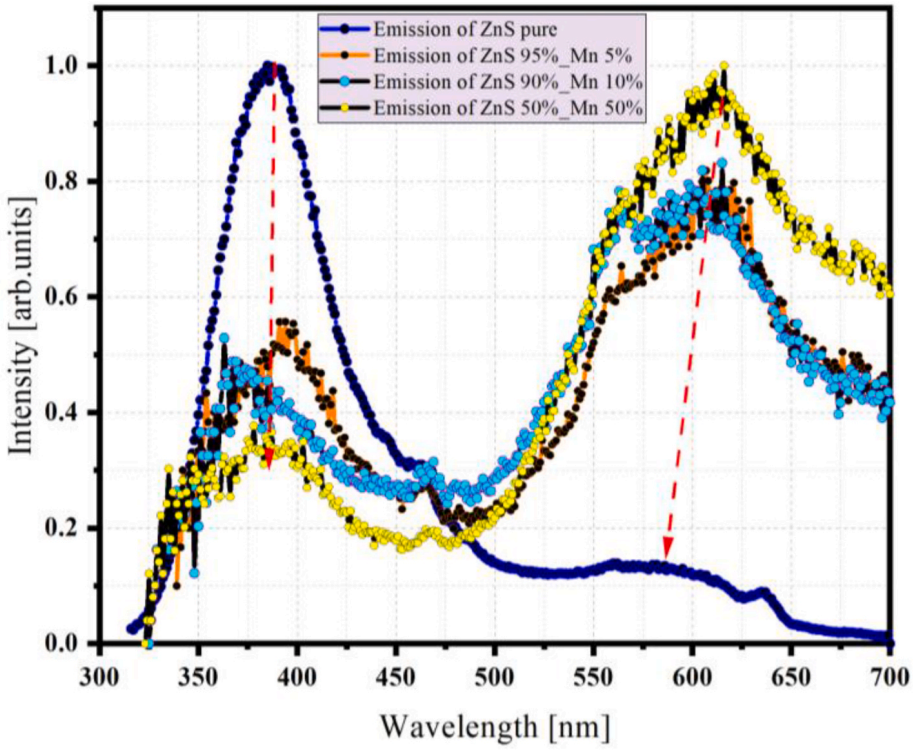


Fig. 17. Emission luminescence spectrum of ZnS thin films doped Mn.

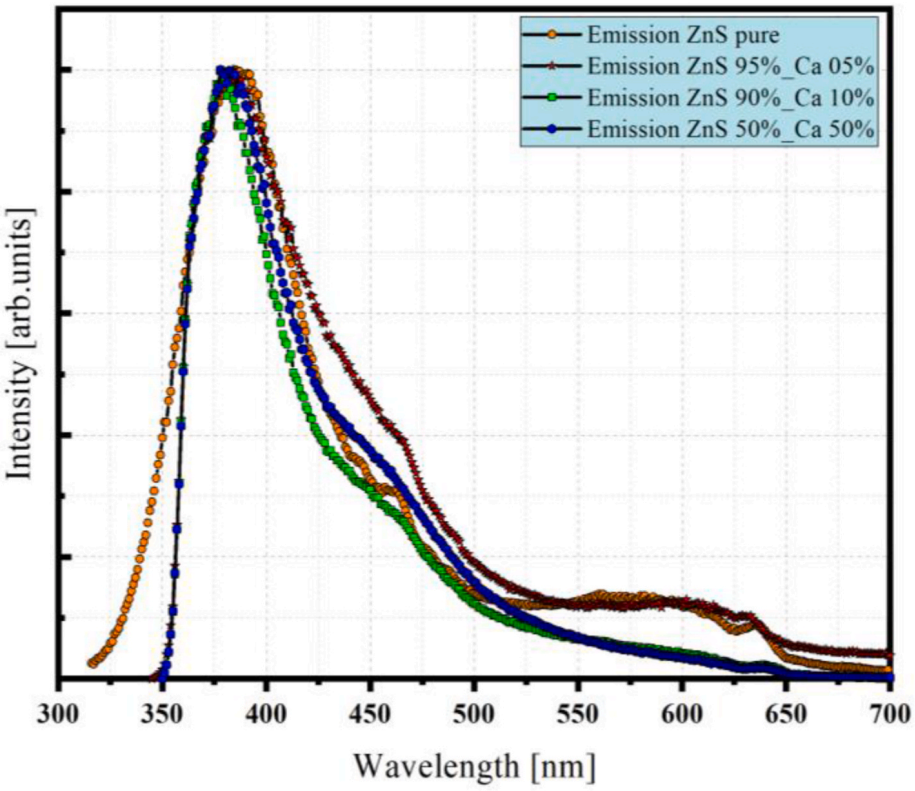


Fig. 18. 3D excitation-emission luminescence spectrum ZnS thin films doped Ca.

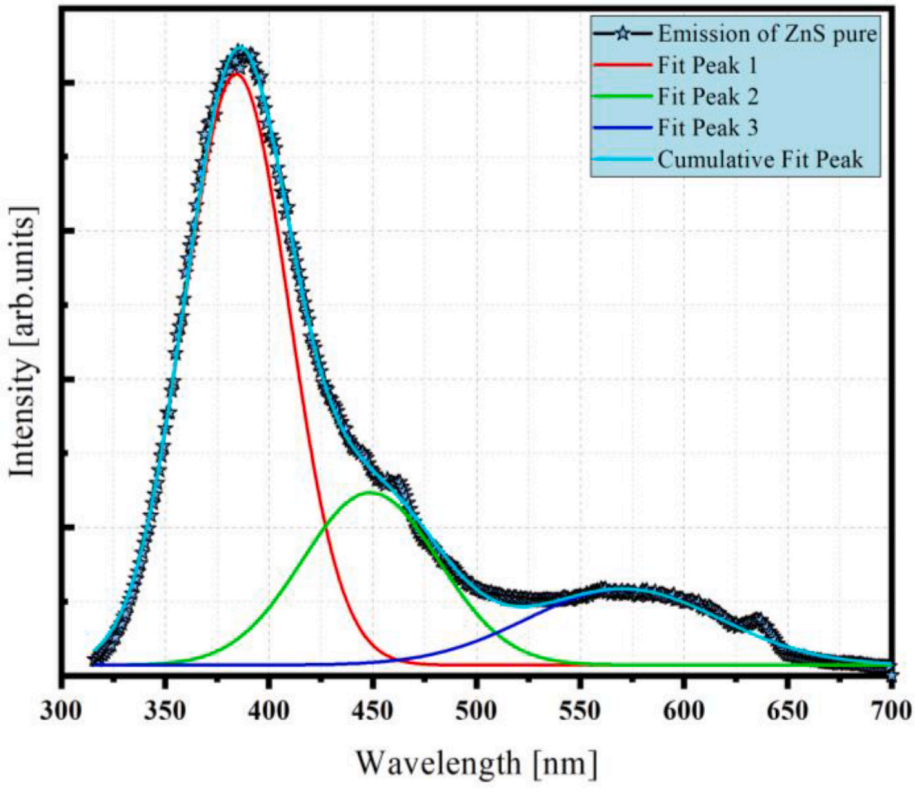


Fig. 19. Emission spectra with Curves fitting at room temperature of pure ZnS thin film.

Table 4
The table groups the values of gap energies obtained by the Tauc plot method for all samples.

	Pure ZnS	Mn			Ca		
		05%	10%	50%	05%	10%	50%
Peak 1 (nm)	385	387	383	385	384	385	386
Peak 2 (nm)	448	457	465	467	440	445	430
Peak 3 (nm)	560	556	552	550	525	520	520
Peak 4 (nm)	–	596	603	614	586	596	592

attributes to thin films. These include variations in film morphology, stoichiometry, and defect density compared to alternative deposition methods.

3.3.2. *Photoluminescence spectroscopy*

Photoluminescence (PL) spectroscopy is a powerful technique that can be used to investigate the electronic and optical properties of materials. The photoluminescence spectra of undoped ZnS, ZnS–Mn, and ZnS–Ca thin films were measured at room temperature. Figs. 17 and 18 present the Emission luminescence spectrum for the investigated samples. A wavelength of 280 nm was selected as the excitation for ZnS thin

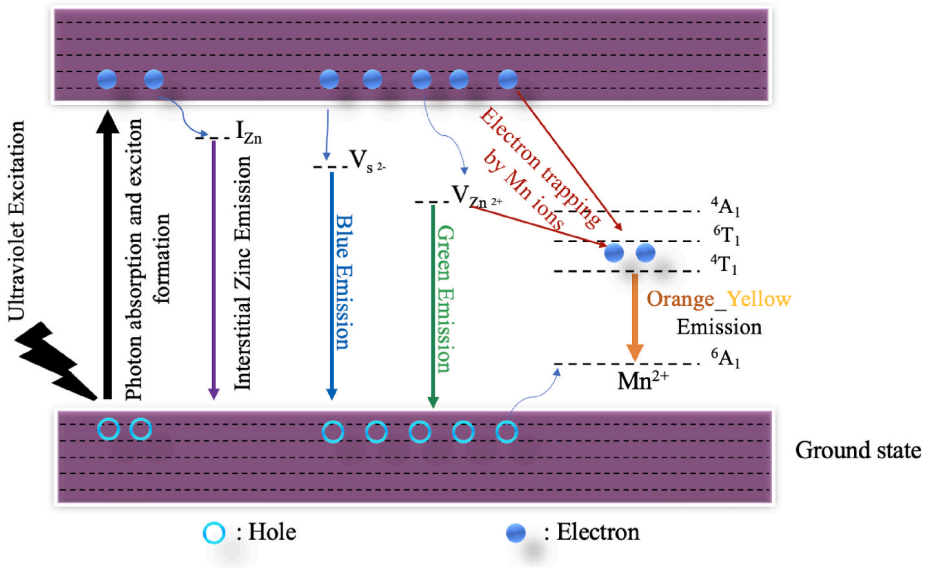


Fig. 20. The schematic energy level mechanism of the ZnS thin films doped Mn.

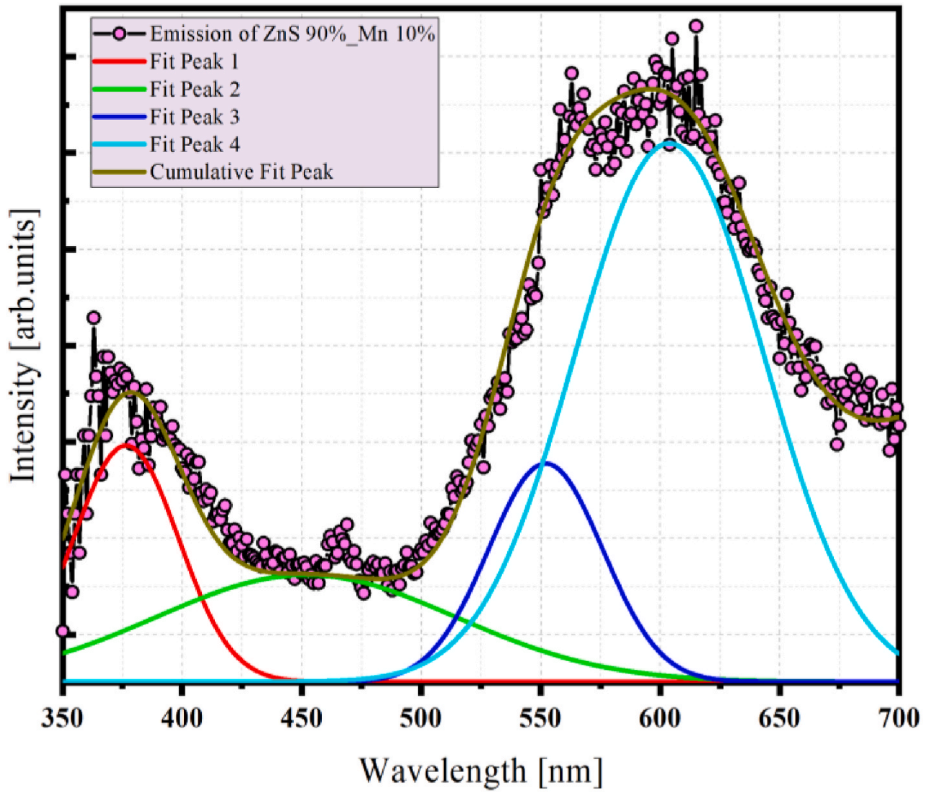


Fig. 21. Emission spectra with Curves fitting at room temperature of 90%ZnS_10% Mn thin film.

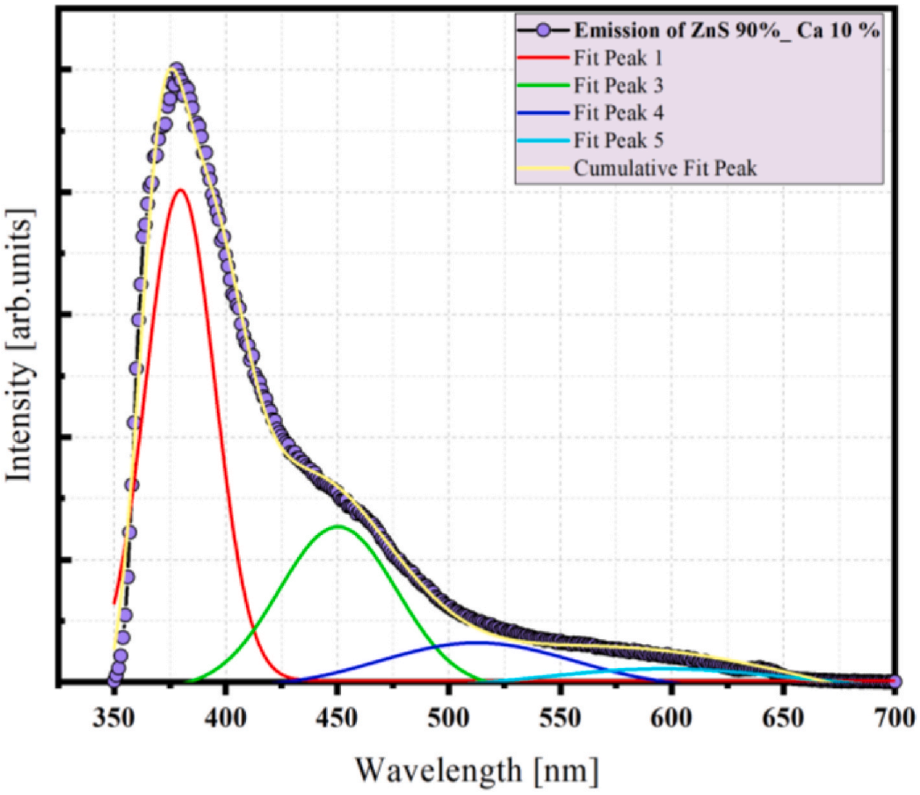


Fig. 22. Emission spectra with Curves fitting at room temperature of 90%ZnS_10% Ca thin film.

Table 5
The CIE (x, y) chromaticity coordinates.

	x_i	y_i
Pure ZnS	0,25	0,24
95% ZnS_05% Mn	0,38	0,45
90% ZnS_10% Mn	0,31	0,46
50% ZnS_50% Mn	0,41	0,48
95% ZnS_05% Ca	0,24	0,24
90% ZnS_10% Ca	0,18	0,18
50% ZnS_50% Ca	0,19	0,16

films doped manganese, while thin films doped calcium were excited at 320 nm.

To investigate carefully the transitions that occurred in the samples, the emission spectra were fitted by using the Gaussian function, Figs. 19, 21 and 22 present curves fitting spectra at room temperature of the elaborated simples. Deconvolution of the emission spectrum of pure ZnS resulted in peaks at 385 nm associated with a UV emission, 448 nm associated with the blue band emission, and 560 nm associated with the green band emission [61,62]. However, it is known from the literature that the PL emission peaks around 385 nm, 448 nm, and 560 nm are often found in ZnS thin films and originate from defects, zinc vacancies, sulfur vacancies, and also from massive defects [63–66]. The characteristic peaks of ZnS are observed in the films with different compositions of Ca and Mn with a shift of the first peak around 2 nm, while the second and third peaks are shifted around 20 nm, as shown in Table 4.

Mn-doped thin films exhibit a fourth peak in the yellow/orange range. The position of this peak shifts towards the red range as the percentage of Mn in the structure increases, and this may be due to the effect of more defects and more strain and stress as a result of the increased Mn concentration as presented in Fig. 17. These peaks correspond to the characteristic $^4T_1 \rightarrow {}^6A_1$ transition of Mn^{2+} ions [67–69]. The doping of ZnS thin films with Mn^{2+} produces intermediate energy levels between the conduction band and the valence band of ZnS Fig. 20 [70,71]. These intermediary energy levels take part in the transition process, resulting in the emission of yellow/orange light with a maximum wavelength of around 614 nm for a sample doped 50% of Mn. This result indicates clearly that the Mn^{2+} ions have been combined successfully with the ZnS host.

The Ca-doped thin films also exhibit a fourth peak with a very weak intensity which is attributed to the Ca impurity. The maximum position of the peak increases towards the longer wavelengths (orange) by varying the percentage of Ca in the thin film, the same results have been found by Refs. [72–74]. The full-half width (FWHM) maxima of the PL bands associated with Ca broaden with increasing the incorporation of Ca into the structure. These results could be attributed to the disordered crystal structure created by the presence of Ca which has a large ionic radius in the ZnS lattice resulting in a disordered crystal structure.

Using photoluminescence data, we investigated the potential of zinc sulfide thin films for future light-emitting diodes (LEDs). To assess their color properties, we constructed the Commission International DeI'llumination (CIE) chromaticity diagram using PL spectra and calculated the CIE color chromaticity coordinates as presented in Table 5 and Fig. 23.

The analysis revealed that the chromaticity coordinates of pure ZnS are located in the light blue region while increasing calcium in the sample shifted the coordinates towards the blue region. Conversely, increasing manganese in the samples allowed the green-yellow region to be involved, similar results were found by Ref. [75]. This study demonstrates the versatility of ZnS thin films in the broad-spectrum visible region, and by careful design and control of composition and parameters, ZnS thin film structures may be used in blue and green light LEDs [76].

Figs. 24 and 25 illustrate XRF measurements conducted on the samples under investigation. In Fig. 24, XRF spectra reveal the presence of various elements: Zinc (Zn), Calcium (Ca), Manganese (Mn), and Sulfide (S). Analysis indicates that Zinc (Zn) and Sulfide (S) display high intensity in samples containing pure ZnS or those with a significant

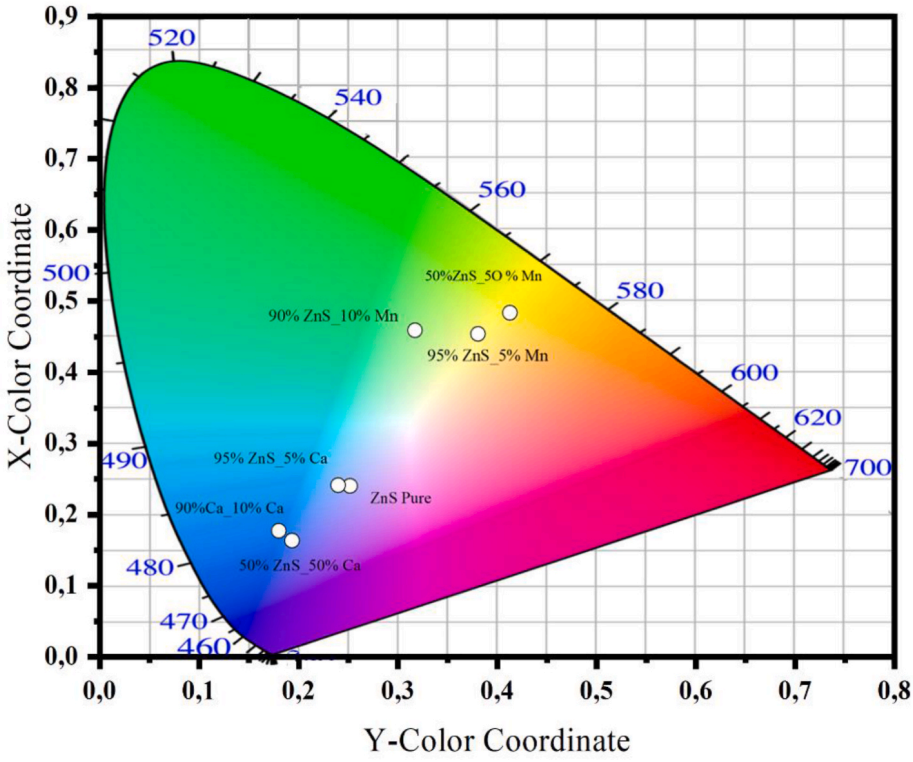


Fig. 23. Chromaticity coordinates of thin films made of pure ZnS and ZnS doped with Mn–Ca.

concentration of these elements, as confirmed by the quantification of Zn and S in the sample shown in Fig. 25.

Conversely, the fluorescence of Manganese (Mn) is more prominent in samples containing 50% Mn, diminishing as the Mn content decreases. A similar trend is observed for Calcium (Ca); however, even in samples devoid of Ca, fluorescence is detected due to Ca present in the glass substrate used for deposition, at a concentration of 6.4%. Therefore, Ca fluorescence is evident in all samples, with higher Ca concentrations corresponding to increased fluorescence intensities. Fig. 25 provides a quantification of all the elements in the samples, with the intensity of peaks for each element reflecting its presence. These results align with the XRF images. Notably, in the sample containing 5% Ca, characteristic Ca peaks are absent due to the similarity in Ca concentration between the sample and the glass substrate, resulting in the absence of Ca peaks after subtracting the substrate response. These results demonstrate that our thin films are deposited with precision, ensuring the presence of the targeted elements.

4. Conclusion

This study provides a comprehensive analysis of the morphological, optical, and photoluminescent properties of zinc sulfide (ZnS) thin films doped with varying concentrations of manganese (Mn) and calcium (Ca). Fabricated using the physical vapor deposition (PVD) method, the films were characterized through various techniques including atomic force microscopy, ultraviolet–visible and photoluminescence, X-ray fluorescence and Fourier transform infrared. The findings indicate that the incorporation of Mn and Ca visibly impacts the surface properties of the thin films, with optical studies demonstrating exceptional transparency within the visible spectrum and a significant decrease in the energy gap due to Ca^{2+} ion inclusion. Moreover, the photoluminescence research revealed significant emission peaks for the samples doped Mn at specific wavelengths, highlighting the material's potential for light emission in response to external stimuli. Additionally, XRF and FTIR analyses confirmed the presence of ZnS and the other elements. The study suggests that PVD is an efficient method for producing Mn and Ca doped ZnS thin films with favorable optical characteristics, holding promise for various optoelectronic applications.

CRediT authorship contribution statement

Amina Laouid: Writing – original draft, Methodology, Investigation, Formal analysis, Data curation. **Amine Alaoui Belghiti:** Validation, Supervision, Investigation, Formal analysis. **Krzysztof Wisniewski:** Methodology, Investigation, Funding acquisition, Formal analysis. **Mohammed Boumhamdi:** Software, Investigation. **Janusz Strzelecki:** Investigation, Funding acquisition, Data curation. **Przemyslaw Plociennik:** Visualization, Validation, Software, Resources. **Abdelowahed Hajjaji:** Writing – review & editing, Visualization, Validation, Supervision. **Anna Zawadzka:** Writing – review & editing, Supervision, Software, Resources, Funding acquisition, Formal analysis.

Declaration of competing interest

The authors declare that they have no known competing financial interests or personal relationships that could have appeared to influence

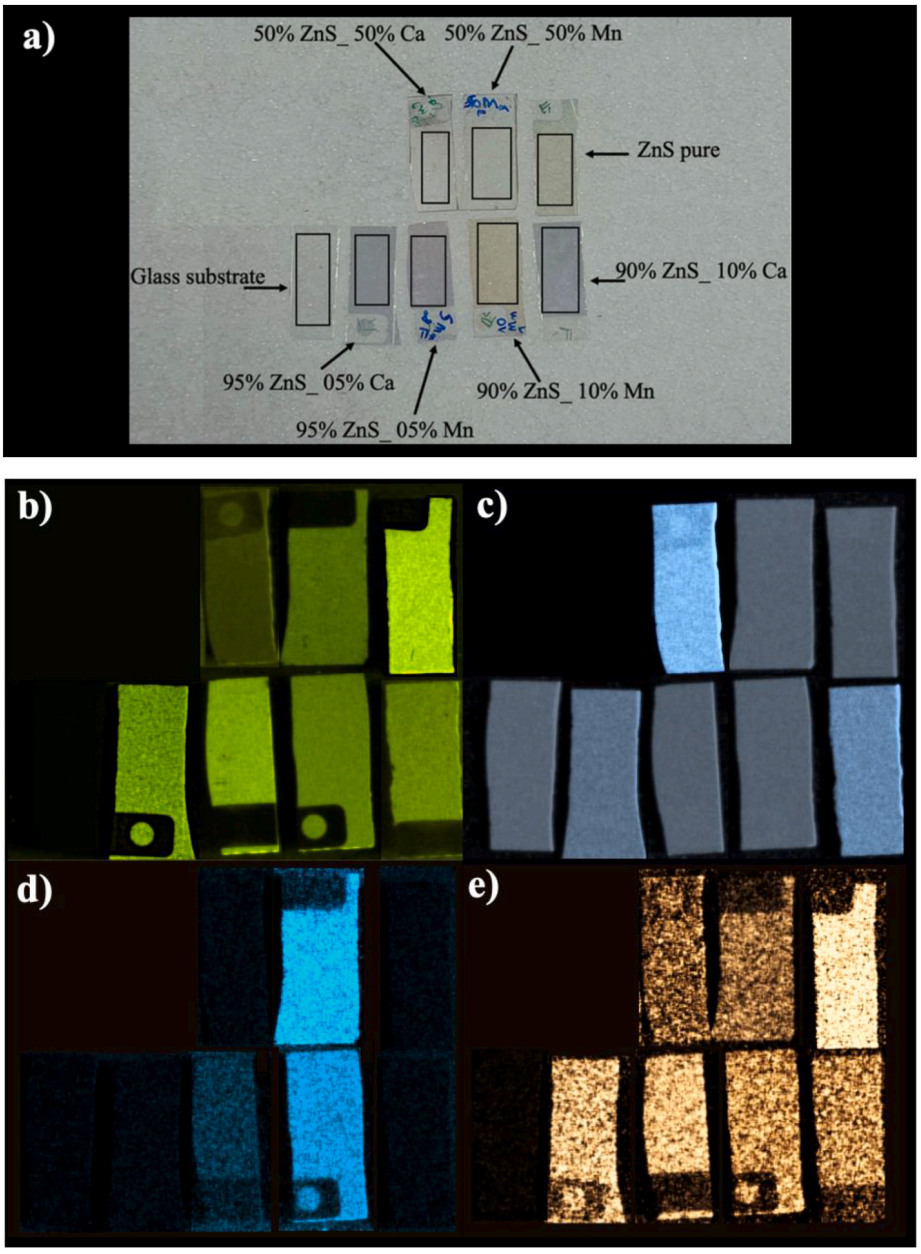


Fig. 24. a) The thin films utilized in the measurement, along with the area examined for XRF analysis b) XRF images of Zinc, c) XRF images of Calcium, d) XRF images of Manganese and e) XRF images of Sulfur.

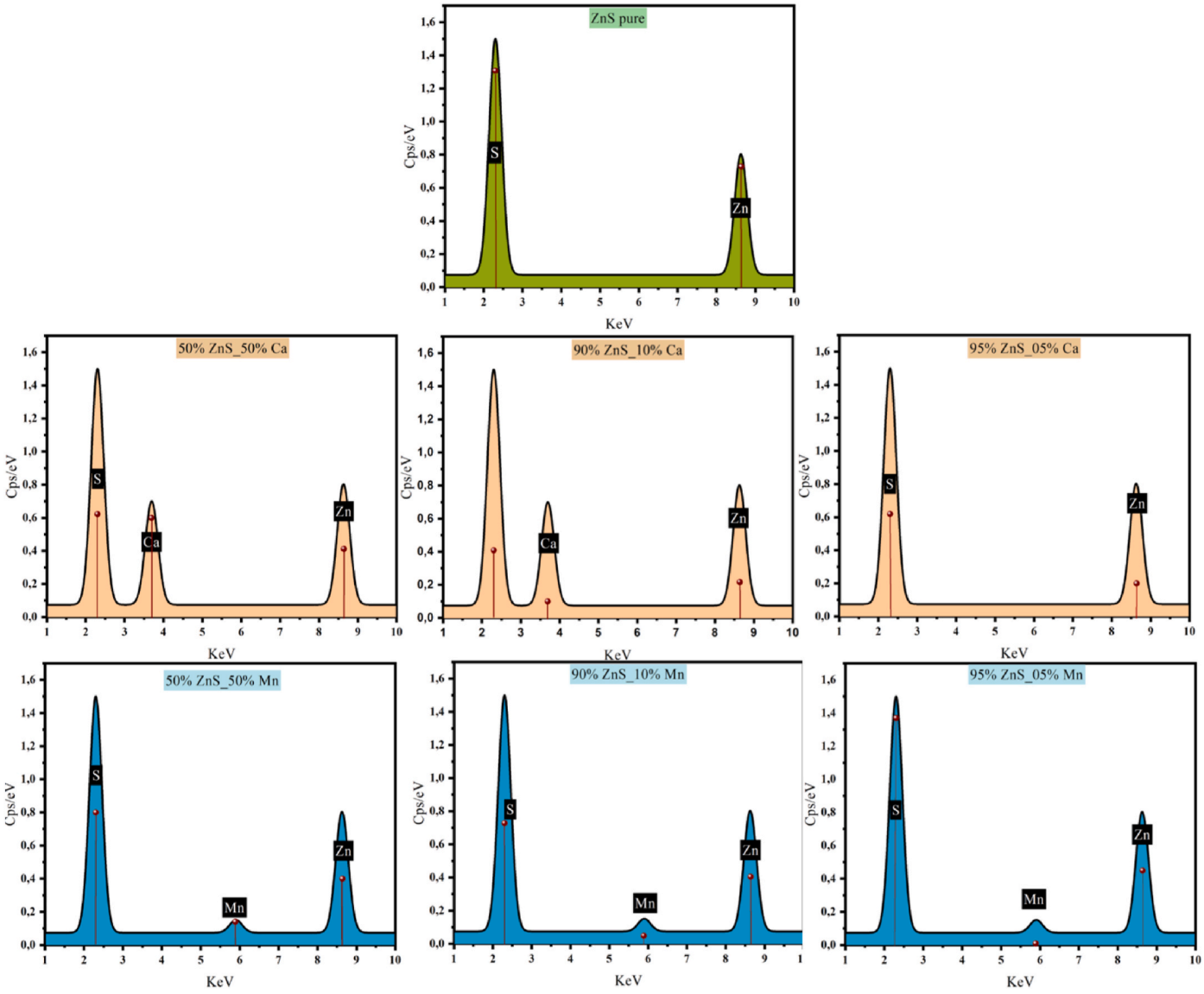


Fig. 25. XFR spectrum for different composition.

the work reported in this paper.

Data availability

Data will be made available on request.

Acknowledgments

This research was financed by the Polish National Science Centre (grant no. 2017/25/B/ST7/02124). Additionally, the films utilized in this study were obtained through the facilities provided by the Interdisciplinary Centre for Modern Technologies at NCU, Torun, Poland. The research was conducted as part of the IDUB NCU project under the emerging research field of 'Material Science and Technology'.

References

[1] K. Ou, S. Wang, G. Wan, M. Huang, Y. Zhang, L. Bai, L. Yi, A study of structural, morphological and optical properties of nanostructured ZnSe/ZnS multilayer thin films, J. Alloys Compd. 726 (2017) 707–711, https://doi.org/10.1016/j.jallcom.2017.08.036.

[2] F. Kurnia, Y.H. Ng, R. Amal, N. Valanoor, J.N. Hart, Defect engineering of ZnS thin films for photoelectrochemical water-splitting under visible light, Sol. Energy Mater. Sol. Cells 153 (2016) 179–185, https://doi.org/10.1016/j.solmat.2016.04.021.

[3] P. Prathap, Y.P.V. Subbaiah, K.T. Ramakrishna Reddy, R.W. Miles, Influence of growth rate on microstructure and optoelectronic behaviour of ZnS films, J. Phys. Appl. Phys. 40 (2007) 5275–5282, https://doi.org/10.1088/0022-3727/40/17/039.

[4] O. El Khouja, I. Boukhoubza, I. Derkaoui, I. Assahsahi, M. Achehboune, A. Talbi, Y. Khaaissa, M. Makha, M. Ebn Touhami, K. Nouneh, Investigation of structural and optical properties of Mg doped ZnS thin films prepared by Mist-CVD technique: experimental and theoretical aspects, Mater. Chem. Phys. 313 (2024) 128707, https://doi.org/10.1016/j.matchemphys.2023.128707.

[5] H.D. Dhaygude, S.K. Shinde, M.V. Takale, G.M. Lohar, M.C. Rath, V.J. Fulari, Effect of electron irradiation on structural, morphological and photoluminescence properties of ZnS thin films, Ceram. Int. 42 (2016) 10159–10164, https://doi.org/10.1016/j.ceramint.2016.03.129.

[6] S. Park, C. Jin, H. Kim, C. Hong, C. Lee, Enhanced violet emission from ZnS nanowires annealed in an oxygen atmosphere, J. Lumin. 132 (2012) 231–235, https://doi.org/10.1016/j.jlumin.2011.08.029.

[7] J. Lee, S. Lee, S. Cho, S. Kim, I.Y. Park, Y.D. Choi, Role of growth parameters on structural and optical properties of ZnS nanocluster thin films grown by solution growth technique, Mater. Chem. Phys. 77 (2003) 254–260, https://doi.org/10.1016/S0254-0584(01)00563-6.

[8] L. Yin, D. Zhang, J. Ma, X. Kong, J. Huang, H. Zhang, C. Liu, Facile synthesis and characterization of ZnS nano/microcrystallites with enhanced photocatalytic activity, Powder Technol. 301 (2016) 1085–1091, https://doi.org/10.1016/j.powtec.2016.07.058.

[9] Y.G. Liu, P. Feng, X.Y. Xue, S.L. Shi, X.Q. Fu, C. Wang, Y.G. Wang, T.H. Wang, Room-temperature oxygen sensitivity of ZnS nanobelts, Appl. Phys. Lett. 90 (2007) 042109, https://doi.org/10.1063/1.2432278.

[10] and and Characterization of ZnS nanoparticles synthesized by co-precipitation method, Chin. Phys. B 24 (2015) 046104, https://doi.org/10.1088/1674-1056/24/4/046104.
[11] S. Muthukumaran, M. Ashok kumar, Structural, FTIR and photoluminescence properties of ZnS:Cu thin films by chemical bath deposition method, Mater. Lett. 93 (2013) 223–225, https://doi.org/10.1016/j.matlet.2012.11.091.
[12] A. Derbali, A. Attaf, H. Saidi, M.S. Aida, H. Benamra, R. Attaf, N. Attaf, H. Ezzaouia, L. Derbali, Br doping effect on structural, optical and electrical properties of ZnS thin films deposited by ultrasonic spray, Mater. Sci. Eng. B 268 (2021) 115135, https://doi.org/10.1016/j.mseb.2021.115135.
[13] S.R. Chalana, R. Jolly Bose, R. Reshmi Krishnan, V.S. Kavitha, R. Sreeja Sreedharan, V.P. Mahadevan Pillai, Structural phase modification in Cu incorporated nanostructured zinc sulfide thin films, J. Phys. Chem. Solids 95 (2016) 24–36, https://doi.org/10.1016/j.jpcs.2016.03.009.
[14] Ş. Uzun Çam, T. Serin, A.N. Yazıcı, Effect of Sn doping concentration on structural, optical and electrical properties of ZnS/p-Si (111) diodes fabricated by sol-gel dip-coating method, Mater. Sci. Semicond. Process. 127 (2021) 105693, https://doi.org/10.1016/j.mssp.2021.105693.
[15] Y. Liu, Y. Sun, W. Liu, J. Yao, Novel high-efficiency crystalline-silicon-based compound heterojunction solar cells: HCT (heterojunction with compound thin-layer), Phys. Chem. Chem. Phys. 16 (2014) 15400–15410, https://doi.org/10.1039/C4CP00668B.
[16] J. Cao, J. Yang, Y. Zhang, L. Yang, Y. Wang, M. Wei, Y. Liu, M. Gao, X. Liu, Z. Xie, Optimized doping concentration of manganese in zinc sulfide nanoparticles for yellow-orange light emission, J. Alloys Compd. 486 (2009) 890–894, https://doi.org/10.1016/j.jallcom.2009.07.097.
[17] Z. Yang, Q. Wu, X. Zhou, F. Cao, X. Yang, J. Zhang, W. Li, A seed-mediated and double shell strategy to realize large-size ZnSe/ZnS/ZnS quantum dots for high color purity blue light-emitting diodes, Nanoscale 13 (2021) 4562–4568, https://doi.org/10.1039/D0NR05025C.
[18] S. Park, S. An, Y. Mun, C. Lee, UV-activated gas sensing properties of ZnS nanorods functionalized with Pd, Curr. Appl. Phys. 14 (2014) S57–S62, https://doi.org/10.1016/j.cap.2013.11.041.
[19] S. Vasilyev, V. Smolski, J. Peppers, I. Moskalev, M. Mirov, Y. Barnakov, S. Mirov, V. Gapontsev, Middle-IR frequency comb based on Cr:ZnS laser, Opt Express 27 (2019) 35079–35087, https://doi.org/10.1364/OE.27.035079.
[20] M.M. Islam, S. Ishizuka, A. Yamada, K. Sakurai, S. Niki, T. Sakurai, K. Akimoto, CIGS solar cell with MBE-grown ZnS buffer layer, Sol. Energy Mater. Sol. Cells 93 (2009) 970–972, https://doi.org/10.1016/j.solmat.2008.11.047.
[21] R. Sahraei, S. Darafarin, An investigation on optical characteristics of nanocrystalline ZnS:Ni thin films prepared by chemical deposition method, Spectrochim. Acta. A. Mol. Biomol. Spectrosc. 149 (2015) 941–948, https://doi.org/10.1016/j.saa.2015.05.036.
[22] P. Yang, M. Lü, D. Xü, D. Yuan, G. Zhou, Photoluminescence properties of ZnS nanoparticles co-doped with Pb2+ and Cu2+, Chem. Phys. Lett. 336 (2001) 76–80, https://doi.org/10.1016/S0009-2614(01)00038-0.
[23] K. Bera, S. Saha, P. Chandra Jana, Investigation of Structural and Electrical properties of ZnS and Mn doped ZnS nanoparticle, Mater. Today Proc. 5 (2018) 6321–6328, https://doi.org/10.1016/j.matpr.2017.12.241.
[24] D.E. Ortíz-Ramos, L.A. González, R. Ramirez-Bon, p-Type transparent Cu doped ZnS thin films by the chemical bath deposition method, Mater. Lett. 124 (2014) 267–270, https://doi.org/10.1016/j.matlet.2014.03.082.
[25] H. Wan, L. Xu, W.-Q. Huang, G.-F. Huang, C.-N. He, J.-H. Zhou, P. Peng, Band engineering of ZnS by codoping for visible-light photocatalysis, Appl. Phys. A 116 (2014) 741–750, https://doi.org/10.1007/s00339-014-8580-3.
[26] X.X. Li, Z. Chen, G. Du, N. Chen, Q. Yu, Synthesis and photoluminescence properties of Cl−-doped ZnS nanoparticles prepared by a solid-state reaction, Mater. Sci. Eng. B 178 (2013) 917–922, https://doi.org/10.1016/j.mseb.2013.05.003.
[27] S. Yano, R. Schroeder, B. Ullrich, H. Sakai, Absorption and photocurrent properties of thin ZnS films formed by pulsed-laser deposition on quartz, Thin Solid Films 423 (2003) 273–276, https://doi.org/10.1016/S0040-6090(02)01037-4.
[28] M. Sreedhar, I. Neelakanta Reddy, P. Bera, T.S. Shyju, C. Anandan, Studies of Cu-doped ZnS thin films prepared by sputtering technique, Surf. Interface Anal. 49 (2017) 284–290, https://doi.org/10.1002/sia.6130.
[29] T.A. Safeera, N. Johns, E.I. Anila, A.I. Martinez, P.V. Sreenivasan, R. Reshmi, M. Sudhanshu, M.K. Jayaraj, Low temperature fabrication and characterization of wurtzite structured ZnS quantum dots by chemical spray pyrolysis, J. Anal. Appl. Pyrolysis 115 (2015) 96–102, https://doi.org/10.1016/j.jaap.2015.07.005.
[30] O.A. Lipina, R.A. Gagarin, L.N. Maskaeva, V.F. Markov, V.I. Voronin, Effect of copper doping on luminescent characteristics of chemically deposited ZnS thin films, AIP Conf. Proc. 2063 (2019) 040034, https://doi.org/10.1063/1.5087366.
[31] A. Tounsi, D. Talantikite-Touati, H. Merzouk, H. Haddad, R. Khalfi, Study of the properties of La-doped ZnS thin Films synthesized by Sol-gel method, Adv. Mater. Lett. 9 (2018) 216–219, https://doi.org/10.5185/amlett.2018.1963.
[32] N. Arbi, I. Ben Assaker, M. Gannouni, A. Kriaa, R. Chtourou, Experimental investigation of the effect of Zn/S molar ratios on the physical and electrochemical properties of ZnS thin films, Mater. Sci. Semicond. Process. 40 (2015) 873–878, https://doi.org/10.1016/j.mssp.2015.07.084.
[33] S. Martínez-Martínez, S.A. Mayén-Hernández, F. de Moure-Flores, MaC. Arenas-Arrocena, E. Campos-González, M.A. Zamora-Antuñano, V.M. Arellano-Badillo, J. Santos-Cruz, Sulfiding effects on ZnS thin films obtained by evaporation technique, Vacuum 130 (2016) 154–158, https://doi.org/10.1016/j.vacuum.2016.05.011.
[34] K. Benyahia, A. Benhaya, M.S. Aida, ZnS thin films deposition by thermal evaporation for photovoltaic applications, J. Semicond. 36 (2015) 103001, https://doi.org/10.1088/1674-4926/36/10/103001.
[35] A. Axelevitch, B. Apter, Preparation and study of doped ZnS thin films, Microelectron. Eng. 170 (2017) 39–43, https://doi.org/10.1016/j.mee.2016.12.027.
[36] R.K. Choubey, S. Kumar, C.W. Lan, Shallow chemical bath deposition of ZnS buffer layer for environmentally benign solar cell devices, Adv. Nat. Sci. Nanosci. Nanotechnol. 5 (2014) 025015, https://doi.org/10.1088/2043-6262/5/2/025015.
[37] S. Gupta, A. Kumar, S. Mukherjee, K.K. Kushwah, S.K. Mahobia, P. Patharia, A. Kushwaha, D. Yadav, U.K. Dwivedi, S. Kumar, R.K. Choubey, Temperature-dependent study of the fabricated ZnS/p-Si heterojunction, Phys. B Condens. Matter 657 (2023) 414831, https://doi.org/10.1016/j.physb.2023.414831.
[38] A. Kumar, S. Mukherjee, H. Sharma, U.K. Dwivedi, S. Kumar, R.K. Gangwar, R. K. Choubey, Role of deposition parameters on the properties of the fabricated heterojunction ZnS/p-Si Schottky diode, Phys. Scr. 97 (2022) 045819, https://doi.org/10.1088/1402-4896/ac6078.
[39] V. Choudapur, S. Kapatkar, A.B. Raju, Structural and optoelectronic properties of zinc sulfide thin films synthesized by Co-precipitation method, Acta Chem. Iasi 27 (2019) 287–302, https://doi.org/10.2478/achi-2019-0018.
[40] A Review on Zinc Sulphide Thin Film Fabrication for Various Applications Based on Doping Elements, (n.d.). https://www.scirp.org/journal/paperinformation?paperid=86917 (accessed February 22, 2024).
[41] A. Laouid, A. Alaoui Belghiti, K. Wisniewski, A. Hajjaji, A. Zawadzka, Structural and optical properties of DCM thin films prepared by PVD, Mater. Today Proc. (2022), https://doi.org/10.1016/j.matpr.2022.03.244.
[42] A. Zawadzka, K. Waszkowska, A. Karakas, P. Płóciennik, A. Korcala, K. Wisniewski, M. Karakaya, B. Sahraoui, Diagnostic and control of linear and nonlinear optical effects in selected self-assembled metallophthalocyanine chlorides nanostructures, Dyes Pigments 157 (2018) 151–162, https://doi.org/10.1016/j.dyepig.2018.04.048.
[43] A. Zawadzka, A. Marjanowska, P. Płóciennik, A. Korcala, K. Wiśniewski, B. Sahraoui, Properties and applications of hybrid organic-inorganic halide perovskites thin films, in: Org. Photonic Mater. Devices XXII, 2020, pp. 59–65, https://doi.org/10.1117/12.2545957. SPIE.
[44] A. Laouid, A. Alaoui Belghiti, K. Wisniewski, J. Strzelecki, A. Karakas, A. Gozutok, Y. El kouari, A. Bouich, M. Tlemçani, P. Plociennik, A. Hajjaji, A. Zawadzka, Optical and morphological properties of DCM thin films co-doped of Znq2 by PVD: theoretical and experimental investigations, Vacuum 222 (2024) 112997, https://doi.org/10.1016/j.vacuum.2024.112997.
[45] I. El Ouedghiri-Idrissi, Z. Sofiani, A. Laouid, A. Talbi, A. Tarbi, Y. El Kouari, A. Zawadzka, Experimental and theoretical study on the optical and morphological properties of highly photoluminescent material 2,4,5-triphenyl imidazole, Opt. Quantum Electron. 56 (2024) 491, https://doi.org/10.1007/s11082-023-06186-6.
[46] A. Marjanowska, H. El Karout, D. Guichaoua, B. Sahraoui, P. Płóciennik, A. Zawadzka, Topography and nonlinear optical properties of thin films containing iodide-based hybrid perovskites, Nanomaterials 14 (2023) 50, https://doi.org/10.3390/nano14010050.
[47] Y. Bouznit, Y. Beggah, M. Wang, N. Tabet, Co-sprayed manganese doped zinc sulfide films, J. Lumin. 151 (2014) 76–81, https://doi.org/10.1016/j.jlumin.2014.02.006.
[48] J. Wang, J. Zhang, S. Li, D. Liu, A. Bhambhani, H. Zeng, Characterization of structures and molecular interactions of RNA and lipid carriers using atomic force microscopy, Adv. Colloid Interface Sci. 313 (2023) 102855, https://doi.org/10.1016/j.cis.2023.102855.
[49] A. Laouid, A.A. Belghiti, K. Wisniewski, A. Hajjaji, B. Sahraoui, A. Zawadzka, Generation of red light with intense photoluminescence assisted by Forster resonance energy transfer from Znq2 and DCM thin films, Environ. Sci. Pollut. Res. (2022), https://doi.org/10.1007/s11356-022-23217-z.
[50] M. Jothibas, s Jeyakumar, C. Manoharan, I. Punithavathy, P. Praveen, P. Richard, Structural and optical properties of zinc sulphide nanoparticles synthesized via solid state reaction method, J. Mater. Sci. Mater. Electron. 28 (2017), https://doi.org/10.1007/s10854-016-5740-6.
[51] C. Sabitha, K.D.A. Kumar, S. Valanarasu, A. Saranya, I.H. Joe, Cu:ZnS and Al:ZnS thin films prepared on FTO substrate by nebulized spray pyrolysis technique, J. Mater. Sci. Mater. Electron. 29 (2018) 4612–4623, https://doi.org/10.1007/s10854-017-8412-2.
[52] A. Jrad, W. Naffouti, T. Ben Nasr, S. Ammar, N. Turki-Kamoun, Effect of manganese concentration on physical properties of ZnS:Mn thin films prepared by chemical bath deposition, J. Mater. Sci. Mater. Electron. 28 (2017) 1463–1471, https://doi.org/10.1007/s10854-016-5682-z.
[53] A. Djelloul, M. Adnane, Y. Larbah, T. Sahraoui, Z. Chewki, A. Maha, B. Rahal, Properties Study of ZnS Thin Films Prepared by Spray Pyrolysis Method, 2015.
[54] B. Jain, A.K. Singh, H. Kim, E. Lichtfouse, V.K. Sharma, Treatment of organic pollutants by homogeneous and heterogeneous Fenton reaction processes, Environ. Chem. Lett. 16 (2018) 947–967, https://doi.org/10.1007/s10311-018-0738-3.
[55] H.M.M.N. Hennayaka, H.S. Lee, Structural and optical properties of ZnS thin film grown by pulsed electrodeposition, Thin Solid Films 548 (2013) 86–90, https://doi.org/10.1016/j.tsf.2013.09.011.
[56] M. Özkan, N. Ekem, S. Pat, M.Z. Balbağ, ZnS thin film deposition on Silicon and glass substrates by Thermionic vacuum Arc, Mater. Sci. Semicond. Process. 15 (2012) 113–119, https://doi.org/10.1016/j.mssp.2011.07.004.
[57] L. Zhou, N. Tang, S. Wu, Influence of deposition temperature on ZnS thin film performance with chemical bath deposition, Surf. Coat. Technol. 228 (2013) S146–S149, https://doi.org/10.1016/j.surfcoat.2012.06.080.

[58] F. Haque, K.S. Rahman, M.A. Islam, M.J. Rashid, M.M. Alam, Z.A. Alothman, K. Sopian, GROWTH OPTIMIZATION OF ZnS THIN FILMS BY RF MAGNETRON SPUTTERING AS PROSPECTIVE BUFFER LAYER IN THIN FILM SOLAR, (n.d.).
[59] C.-M. Huang, L.-C. Chen, G.-T. Pan, T.C.K. Yang, W.-S. Chang, K.-W. Cheng, Effect of Ni on the growth and photoelectrochemical properties of ZnS thin films, Mater. Chem. Phys. 117 (2009) 156–162, https://doi.org/10.1016/j.matchemphys.2009.05.026.
[60] I.-D. Simandan, F. Sava, A.-T. Buruiana, I. Burducea, N. Becherescu, C. Mihai, A. Velea, A.-C. Galca, The effect of the deposition method on the structural and optical properties of ZnS thin films, Coatings 11 (2021) 1064, https://doi.org/10.3390/coatings11091064.
[61] Nasser Saad Al-Din -Abalh Alzoubi, Zeinab Alhassan, Albaath universty, Study of the effect of different dopants on optical properties of ZnS thin films, Int. J. Eng. Res. V9 (2020), https://doi.org/10.17577/IJERTV9IS020271. IJERTV9IS020271.
[62] R. Khan, N.S. Das, K.K. Chattopadhyay, Cathodoluminescence and photoluminescence from ZnS thin films deposited by novel seeded hydrothermal route, J. Mater. Sci. Mater. Electron. 30 (2019) 19189–19198, https://doi.org/10.1007/s10854-019-02276-y.
[63] P. Roy, J.R. Ota, S.K. Srivastava, Crystalline ZnS thin films by chemical bath deposition method and its characterization, Thin Solid Films 515 (2006) 1912–1917, https://doi.org/10.1016/j.tsf.2006.07.035.
[64] N. Saravanan, G.B. Teh, S.Y.P. Yap, K.M. Cheong, Simple synthesis of ZnS nanoparticles in alkaline medium, J. Mater. Sci. Mater. Electron. 19 (2008) 1206–1208, https://doi.org/10.1007/s10854-007-9529-5.
[65] D. Kurbatov, V. Kosyak, A. Opanasyuk, V. Melnik, Native point defects in ZnS films, Phys. B Condens. Matter 404 (2009) 5002–5005, https://doi.org/10.1016/j.physb.2009.08.197.
[66] C. Chen, J. Zhu, Y. Zhang, A. Wang, Preparation and luminescence properties of PVDF/ZnS:Mn flexible thin-film sensors, Coatings 12 (2022) 449, https://doi.org/10.3390/coatings12040449.
[67] P.D. Angelo, R. Kronfli, R.R. Farnood, Synthesis and inkjet printing of aqueous ZnS: Mn nanoparticles, J. Lumin. 136 (2013) 100–108, https://doi.org/10.1016/j.jlumin.2012.10.043.
[68] M.R. Kim, J.H. Chung, D.-J. Jang, Spectroscopy and dynamics of Mn2+ in ZnS nanoparticles, Phys. Chem. Chem. Phys. 11 (2009) 1003–1006, https://doi.org/10.1039/b813452a.
[69] M. Hossu, R.O. Schaeffer, L. Ma, W. Chen, Y. Zhu, R. Sammynaiken, A.G. Joly, On the luminescence enhancement of Mn2+ by co-doping of Eu2+ in ZnS:Mn,Eu, Opt. Mater. 35 (2013) 1513–1519, https://doi.org/10.1016/j.optmat.2013.03.014.
[70] V. Proshchenko, Y. Dahnovsky, Long-lived emission in Mn doped CdS, ZnS, and ZnSe diluted magnetic semiconductor quantum dots, Chem. Phys. 461 (2015) 58–62, https://doi.org/10.1016/j.chemphys.2015.09.001.
[71] K. Kavi Rasu, P. Sakthivel, G.K.D. Prasanna Venkatesan, Effect of Pd2+ co-doping on the structural and optical properties of Mn2+:ZnS nanoparticles, Opt Laser. Technol. 130 (2020) 106365, https://doi.org/10.1016/j.optlastec.2020.106365.
[72] S. Kar, S. Chaudhuri, Controlled synthesis and photoluminescence properties of ZnS nanowires and nanoribbons, J. Phys. Chem. B 109 (2005) 3298–3302, https://doi.org/10.1021/jp045817j.
[73] L. Tairi, Y. Messai, R. Bourzami, A. Chetoui, M. Sebais, T. Tahraoui, T. Bouarroudj, H. Bezzi, D.E. Mekki, Enhanced photoluminescence and photocatalytic activity of Ca2+ addition into ZnS nanoparticles synthesized by hydrothermal method, Phys. B Condens. Matter 631 (2022) 413713, https://doi.org/10.1016/j.physb.2022.413713.
[74] A.S. Messalti, M. El-Ghozzi, D. Zambon, R. Mahiou, Z. Setifi, Investigating photoluminescence properties of Ca-doped ZnS nanoparticles prepared via hydrothermal method, J. Lumin. 238 (2021) 118227, https://doi.org/10.1016/j.jlumin.2021.118227.
[75] A. Kumar, S. Mukherjee, H. Sharma, D.K. Rana, A. Kumar, R. Kumar, R.K. Choubey, Fabrication of low-cost and fast-response visible photodetector based on ZnS:Mn/p-Si heterojunction, Mater. Sci. Semicond. Process. 155 (2023) 107226, https://doi.org/10.1016/j.mssp.2022.107226.
[76] A. Kumar, M. Kumar, V. Bhatt, D. Kim, S. Mukherjee, J.-H. Yun, R.K. Choubey, ZnS microspheres-based photoconductor for UV light-sensing applications, Chem. Phys. Lett. 763 (2021) 138162, https://doi.org/10.1016/j.cplett.2020.138162.